Cell Biol Toxicol (2025) 41:3
https://doi.org/10.1007/s10565-024-09946-6

RESEARCH

miR-21-loaded bone marrow mesenchymal stem cell-derived exosomes inhibit pyroptosis by targeting MALT1 to repair chemotherapy-induced premature ovarian insufficiency

Lichao Tang · Yutao Yang · Mingxin Yang · Jiaxin Xie · Aiping Zhuo · Yanhong Wu · Mengli Mao · Youhong Zheng · Xiafei Fu

Received: 29 June 2024 / Accepted: 7 November 2024

Abstract Chemotherapy is essential for treating malignant tumors, but it can cause premature ovarian insufficiency (POI). Recent studies suggest that exosomes enriched with miR-21 (miR-21-Exo) may help mitigate POI, though the underlying mechanisms remain largely unexplored. This research investigates how miR-21-Exo influences chemotherapy-induced POI using an experimental model where KGN cells are exposed to cisplatin. We assessed the impact of miR-21 on cellular activity and generated miR-21 overexpressing bone marrow mesenchymal stem cells (miR-21-BMSC) via lentiviral modification. Isolated miR-21-Exo was analyzed for its effects on cellular function. Bioinformatics identified Mucosa-Associated Lymphoid Tissue Lymphoma Translocation Protein 1 (MALT1) as a target of miR-21. We confirmed that miR-21-Exo regulates MALT1 and the NF-κB signaling pathway to prevent cell pyroptosis. Further studies in a rat model demonstrated the therapeutic potential and safety of miR-21-Exo. Overall, our findings highlight a novel strategy for addressing chemotherapy-induced POI by modulating MALT1 and the NF-κB pathway, offering significant therapeutic implications.

Keywords Premature ovarian insufficiency · MiR-21 · Bone mesenchymal stem cell · Exosome · MALT1 · Pyroptosis

Introduction

Premature ovarian insufficiency (POI) is a medical condition characterized by diminished ovarian function occurring prior to the age of 40 (Webber et al. 2016). The primary clinical manifestations of this disorder include irregular or absent menstruation, infertility, episodes of sudden intense heat, and symptoms related to osteoporosis. The etiology of POI encompasses multiple factors, including genetic predisposition, immunological disorders, iatrogenic causes, and environmental influences (Rebar 2009). In recent years, there has been a steady increase in tumor incidence, with chemotherapy serving as a primary treatment method for various malignant tumors. Although chemotherapy can effectively eliminate cancer cells, its adverse effects may damage ovarian tissues and reduce the number of ovarian follicles, ultimately resulting in chemotherapy-induced POI (Tsiligiannis et al. 2019).

Lichao Tang and Yutao Yang are co-authors.

Supplementary Information The online version contains supplementary material available at https://doi.org/10.1007/s10565-024-09946-6.

L. Tang · Y. Yang · M. Yang · J. Xie · A. Zhuo · Y. Wu · M. Mao · Y. Zheng · X. Fu (✉)
Department of Obstetrics and Gynecology, Zhujiang Hospital, Southern Medical University, Guangzhou, Guangdong, China
e-mail: fxf1997@smu.edu.cn

Published online: 20 December 2024

Pyroptosis is classified as a type of programmed cell death (Rao et al. 2022).The activation of cysteine-aspartic proteases, particularly Caspase-1 (CASP1), within the inflammasome results in the cleavage and aggregation of Gasdermin family members, such as Gasdermin D (GSDMD). This process ultimately leads to the formation of pores in the cell membrane and subsequent cell death(Yu et al. 2021). Researchers observed elevated levels of pyroptosis-related molecules and inflammatory markers in a mouse model of chemotherapy-induced POI compared to mice without the condition (Miao et al. 2023). Moxibustion effectively enhances ovarian reserve in chemotherapy-induced POI rats by suppressing the NLRP3 pathway (Yin et al. 2023). Suppressing pyroptosis could be a promising strategy for addressing chemotherapy-induced POI. miR-21 is a 22-nucleotide long, single-stranded non-coding short RNA molecule that influences cell proliferation, apoptosis, and differentiation, hence affecting the progression of illnesses (Jenike and Halushka 2021). Research has demonstrated that tracheal epithelial cells secrete extracellular vesicles that contain miR-21-5p. This miRNA has the ability to suppress pyroptosis in alveolar macrophages, hence improving the lung's capacity to defend against bacterial infections (Wang et al. 2024). Prior studies have shown that bone marrow mesenchymal stem cells carrying miR-21 (miR-21-BMSC) show reparative effects on POI both in vitro and in vivo (Yang et al. 2024). Although the specific effects of miR-21 in inhibiting pyroptosis are not yet fully understood.

To successfully deliver miR-21 into cells, researchers have used exosomes for transport. Exosomes are extracellular vesicles that originate from cells and have a size ranging from 50 to 150 nm, containing various biomolecules including proteins and nucleic acids, acting as carriers involved in various physiological and pathological processes (Meldolesi 2018). Researchers are currently investigating the potential use of exosomes produced from several stem cell sources for the treatment of POI (Liao et al. 2021). These exosomes may regulate ovarian tissue function, promoting repair and regeneration. Some studies even attempt to load specific molecules into extracellular vesicles to enhance their therapeutic effects (Cai et al. 2022; Ding et al. 2020a, b; Ding et al. 2020a, b; Thabet et al. 2020; Yang et al. 2020).

This research hypothesizes that exosomes derived from bone marrow mesenchymal stem cells carrying miR-21 can inhibit granulosa cell pyroptosis in chemotherapy-induced POI by targeting MALT1. This discovery may provide a novel therapeutic approach for managing POI.

Materials and methods

Cell lines and cell culture

Procell Life Science & Technology in China provided mouse BMSC and the human granulosa-like tumor cell line KGN. The Translational Medicine Research Center at Zhujiang Hospital in China provided the HEK293T cells. The culture media used for BMSC was Dulbecco's modified Eagle's medium (DMEM)/F12 medium (Gibco, USA), which contained 1% penicillin–streptomycin and 10% fetal bovine serum (FBS). KGN cells were grown in DMEM/F12 media (produced in China by KeyGEN BioTECH), which was enhanced with 1% penicillin–streptomycin and 10% foetal bovine serum. 10% FBS and 1% penicillin–streptomycin were added to high-glucose DMEM (KeyGEN BioTECH, China) for the cultivation of HEK293T cells. The incubation was conducted at a temperature of 37 °C in a controlled environment with 95% oxygen and 5% carbon dioxide.

To prepare KGN cells, culture them in dishes and incubate at 37 °C with 5% CO2 for 24 h. Once the adhesion rate reaches 50–70%, randomly assign the cells into four experimental groups: the control group (NC group), the cisplatin-induced damage model group (CDDP group), the group treated with Exo (CDDP + Exo group), and the group treated with miR-21-Exo (CDDP + miR-21-Exo group). The NC group receives no treatment. The CDDP, CDDP + Exo, and CDDP + miR-21-Exo groups are administered 5 mg/L of cisplatin (Jiangsu Haosen Pharmaceutical Group Co., Ltd., China). After 24 h, the cisplatin-containing medium is replaced with fresh medium. The CDDP + Exo and CDDP + miR-21-Exo groups are then incubated for an additional 24 h with 30 μg/mL of Exosomes or miR-21-Exosomes. The CDDP group is given an equivalent volume of phosphate-buffered saline (PBS).

Transfection of cells

A lentiviral vector (LV-hsa-mir-21) from GeneChem (Shanghai) was used to add miR-21 to both KGN cells and BMSC. We used quantitative reverse transcription-polymerase chain reaction (qRT-PCR) to measure the levels of miR-21 in BMSC and their Exo after infection. In the experiment, granulosa cells overexpressing miR-21 (LV-miR-21-KGN) and control granulosa cells (LV-NC-KGN) were treated with or without cisplatin. The experiment was divided into four groups: the empty vector group (LV-NC), the miR-21 virus transfection group (LV-miR-21), the empty vector plus cisplatin group (LV-NC + CDDP), and the miR-21 virus transfection plus cisplatin group (LV-miR-21 + CDDP).

Bioinformatics research showed which genes miR-21 targets and suggested that miR-21 would bind to the 3' untranslated region (UTR) of MALT1 mRNA. There were four separate groups in the rescue tests. These were the NC group, the CDDP group, the CDDP + miR-21-Exo group, and the CDDP + miR-21-Exo + OE-MALT1 group. Before adding the exosomes, transfection was done. The MALT1 overexpression plasmid was created by IGE Biotechnology in China and was made to contain only the coding region. This plasmid was transfected into the CDDP + miR-21-Exo + OE-MALT1 group. Following the manufacturer's instructions, the transfection process was carried out using LipoMax transfection reagent (IGE Biotechnology, China). Using an empty vector plasmid, the NC group, CDDP group, and CDDP + miR-21-Exo group were transfected.

For the 293T cells, the experimental group was transfected with miR-21 mimic, while the control group was transfected with miR-21 NC. The miR-21 mimic and miR-21 NC from IGE Biotechnology in China were used for transfection, along with LipoMax transfection reagent, following the manufacturer's instructions.

The processes of isolating, identifying, labeling, and detecting Exo and miR-21-Exo are performed

To isolate miR-21-Exo or Exo from the serum-free culture supernatants of miR-21-BMSC or BMSC, ultracentrifugation is employed. First, the collected supernatant is centrifuged at 300 g for 10 min, followed by 2000 g for 10 min, and then 10,000 g for 30 min to remove dead cells and debris. The resulting supernatant is then centrifuged at 100,000 g for 70 min to pellet the exosomes. The pellet is resuspended in PBS for further analysis. The morphology of the exosomes is examined using transmission electron microscopy (TEM), their size is measured with a Flow NanoAnalyzer from NanoFCM, and their surface markers are analyzed via western blotting.

The exosomes were labeled with the fluorescent dye 1,1'-dioctadecyl-3,3,3',3'-tetramethylindotricarbocyanine iodide (DiR; Molecular Probes, USA). The labeled exosomes were washed with PBS at 100,000 g for 70 min. They were then co-incubated with CDDP-stimulated KGN cells for 24 h. Afterwards, the KGN cells were treated with a 4% solution of paraformaldehyde to preserve them, and their nuclei were stained with 4',6-diamidino-2-phenylindole (DAPI; Solarbio, China). Nikon produced a confocal microscope that was used to visualize exosome uptake.

Creation of a rat model with chemotherapy-induced POI and administration of Exo or miR-21-Exo by injection

Female Sprague–Dawley (SD) rats, aged 7–8 weeks and weighing 180-220 g, were acquired from the Experimental Animal Center of Southern Medical University. The rats were housed in a regulated environment with a temperature of 30 ± 2 °C and a 12-h cycle of light and darkness. They had unrestricted access to food and water. This study was approved by the Ethics Committee of Zhujiang Hospital, Southern Medical University, accepted this study (Approval No. LAEC-2022–208) and ensured compliance with all ethical criteria.

A total of thirty-two female rats with regular estrous cycles were randomly assigned to four groups: the NC group (n = 8), the POI group (n = 8), the POI + Exo group (n = 8), and the POI + miR-21-Exo group (n = 8). The chemotherapy-induced POI model was established by administering cisplatin solution intraperitoneally at a dosage of 1 mg/kg for a duration of 14 consecutive days (Qu et al. 2022). The rats in the NC group were given an equivalent amount of saline at the identical location.

Successful establishment of the chemotherapy-induced POI model was anticipated 14 days after the completion of cisplatin injections. After receiving cisplatin injections, rats in the Exo and miR-21-Exo

groups were administered injections of 150 μg of Exo or miR-21-Exo, which were dispersed into 1 ml of PBS every other day for a total of 7 injections. In contrast, rats in the POI group were given injections of PBS. After a period of two weeks following the administration of Exo or miR-21-Exo, half of the rats were sacrificed. Samples of serum, ovarian tissue, and other organs including the heart, liver, spleen, lung, kidney, and uterine were obtained. The remaining female SD rats were co-housed in a ratio of two females to one male for 10 days, ensuring that they had enough water and food available. After the co-housing period, female and male rats were separated based on gender. Female rats were monitored for signs of pregnancy and litter size.

Animal imaging conducted in vivo

Following the injection of exosomes for in vivo monitoring, the rats were seen and monitored using the PerkinElmer IVIS Spectrum in vivo imaging system (China) at predetermined intervals of time (1 h, 3 h, 24 h, 48 h, 21 days, and 28 days). Fluorescent pictures showing the movement and distribution of DiR-miR-21-Exo were captured using light with a wavelength of 740 nm to excite the molecules and a wavelength of 790 nm to detect their emission. The images were then analyzed using PerkinElmer's Living Image 4.5.5 program.

Examination of the estrous cycle

Regular vaginal cytology checks were exams were performed to track the estrous cycles on a daily basis. Vaginal secretions were obtained by utilizing a small cotton swab, which was then treated with trypan blue dye (Biosharp, China) and observed using a bright-field upright microscope (Leica, Germany).

The structure and number of ovarian follicles

The ovarian tissue was preserved in 4% PFA for a period of 24 to 48 h and then encased in paraffin. Consecutive sections with a thickness of 5 μm were acquired, subjected to hematoxylin and eosin (H&E) staining, and examined using a 3D scanner.

Follicle counting involved consecutive sectioning with counting every fifth slice to tally the overall quantity of each type of follicle, resulting in a final count multiplied by 5 (Tilly 2003). Each sample group consisted of at least 3 rats for statistical analysis. Subsequently, using 3D scanner software, primordial, primary, secondary, and mature follicles were identified and quantified based on morphological features under 100× magnification.

TUNEL analysis of ovarian

Follicle apoptosis was assessed using the TUNEL assay kit (Elabscience, China). The tissue was sectioned into 5 mm pieces and fixed in paraffin. Images were obtained using a fluorescence microscope after staining with fluorescein isothiocyanate (FITC) and DAPI. The data analysis was conducted using the ImageJ software.

Immunohistochemistry

The paraffin-embedded sections underwent treatment using rabbit polyclonal antibodies against Proliferating Cell Nuclear Antigen (PCNA), NACHT, LRR and PYD domains-containing protein 3 (NLRP3), and GSDMD, all at a dilution of 1:1000. The sections were then stained using secondary antibodies and diaminobenzidine (DAB) reagent. After being submerged in a solution of hematoxylin dye for a duration of 3 min, the sections were rinsed with water and then subjected to a 1-s process of differentiation in hydrochloric acid alcohol. Finally, the sections were incubated in PBS for a period of 1 min.

The proportion of cells that exhibited positive staining was assessed using a 3DHISTECH bright-field scanner from Hungary.

Enzyme-Linked Immunosorbent Assay (ELISA)

In order to identify the existence of estradiol (E_2) in the fluids surrounding the cells, it is more effective to provide the testosterone substrate (Huang et al., 2020). After 48 h, the liquid portion of the cells was gathered, and the levels of estradiol were determined using ELISA kits from R&D Systems, USA. The ELISA kits were utilized to quantify the levels of E_2, Follicle Stimulating Hormone (FSH), and anti-Müllerian hormone (AMH) in serum samples obtained on the 0th day, 28th day, and 42nd day after the initiation of cisplatin injection. A spectrophotometric analysis was performed using a BioTek

microplate reader from the United States to measure the absorbance at a wavelength of 450 nm.

Cell proliferation experiment

We employed the Cell Counting Kit 8 (CCK8; APExBIO, USA) to assess cellular proliferation. The KGN cells were initially placed in a 96-well plastic plate. A 100 µL cell supernatant and a 10 µL CCK8 solution were added to every well. The plate was then kept in an incubator set at a temperature of 37 °C for a pperiod of 1 h. We assessed cell proliferation at 0, 24, 48, 72, and 96 h by measuring absorbance at 450 nm using a microplate reader.

Analysis using fluorescence-activated cell sorting

To detect apoptosis, cells were stained with V-FITC and propidium iodide (V-FITC/PI) using the apoptosis detection kit from Beyotime Biotechnology, China, following the instructions provided by the manufacturer. Fluorescence-activated cell sorting (FACS) was used to sort cells that had been stained.

qRT-PCR Analysis

RNA extraction was performed on cells or half of each mouse ovary using RNAex Pro reagent (Agbio, USA). The process of reverse transcription was conducted using Evo M-MLV RT Premix (Agbio, USA) and 500 ng of RNA. The qRT-PCR analysis was conducted using SYBR Pro Taq HS Premix (Agbio, USA) on a CFX96 Real-Time PCR Detection System (Bio-Rad, USA). U6 was used as the internal control for miR-21, while GAPDH was used as the internal control for Follicle Stimulating Hormone Receptor (FSHR), Cytochrome P450 Family 11 Subfamily A Member 1 (CYP11A1), Cytochrome P450 Family 19 Subfamily A Member 1 (CYP19A1), Hydroxysteroid (17-beta) dehydrogenase 1 (HSD17B1), Steroidogenic Acute Regulatory Protein (STAR), NLRP3, CASP1, GSDMD, and MALT1. The data analysis was performed with the software provided by Bio-Rad. The primer sequences can be found in Supplementary Table 1.

Western blotting

Protease and phosphatase inhibitors were employed in conjunction with RIPA lysis buffer (Cwbio, China) to lyse exosomes, cells, and half of each rat ovary in order to extract proteins. The BCA protein assay kit (Beyotime Biotechnology, China) was utilized to ascertain the protein concentration. Following protein denaturation, electrophoresis was carried out using SDS-PAGE, and the gel was subsequently transferred to a PVDF membrane (Millipore, USA). After transfer, a 5% BSA solution (MCR, China) was used to block the membrane. It was then incubated with particular primary antibodies for an entire night. These antibodies included anti-CD9 (HuaBio, China), anti-TSG101 (HuaBio, China), anti-CD81 (Abmart, China), anti-NLRP3 (Abmart, China), anti-CASP1 (Abmart, China), anti-GSDMD (Abmart, China), anti-pP65 (Abmart, China), anti-pIKK (Abmart, China), anti-pIKB (Abmart, China), (Proteintech, China). Following a 1-h exposure to a secondary antibody from Cwbio (China), the membrane was cleaned using Tris-buffered saline–Tween (TBS-T; Boster, China). The detection technique was carried out using an electrochemiluminescence (ECL) apparatus manufactured by Beyotime Biotechnology in China. The reference standard was glyceraldehyde-3-phosphate dehydrogenase (GAPDH). Using ImageJ software, protein levels were examined. The target protein's relative content in the samples was calculated by dividing its grayscale value by GAPDH's grayscale value.

Dual luciferase reporter gene analysis

The putative mRNA predicted for miR-21 miRNA were identified and compared using the online target prediction algorithms Tarbase (miRNA target gene database, https://dianalab.e-ce.uth.gr/tarbasev9, predicted 1588 miR-21 target genes), miRDB (miRNA target gene predictions, https://mirdb.org/, predicted 469 miR-21 target genes), DIANA tools (Various miRNA analysis tools, https://dianalab.e-ce.uth.gr/html/mirpathv3/index.php?r=mirpath, predicted 515 miR-21 target genes), miRTarBase (miRNA target gene database, primarily based on experimental validation, https://mirtarbase.cuhk.edu.cn/, predicted 625 miR-21 target genes), and miRWalk (miRNA target gene predictions and database, http://mirwalk.umm.

uni-heidelberg.de/, predicted 2214 miR-21 target genes). The 27 genes closely associated with pyroptosis are derived from rectome (https://reactome.org/). The 55 genes that are closely associated with NF-κB signaling are sourced from GeneCards (https://www.genecards.org/).The miRDB website was used to estimate the binding sites of MALT1 and miR-21. The psiCHECK-2 reporter vector containing the wild-type (MALT1-wt) and mutant (MALT1-MUT) MALT1 constructs was used to build the reporter vector for the dual-luciferase reporter gene experiment. The MALT1-WT and MALT1-MUT reporter plasmids were simultaneously introduced into HEK293T cells together with either a miR-21 mimic or a control mimic (IGE Biotechnology, China) using Lipofectamine 3000 (Invitrogen, USA). The luciferase activity was assessed using the Dual-Luciferase Reporter Assay System provided by Beyotime Biotechnology (China) following a 48-h transfection period.

LDH Detection

The supernatant of the cell culture was collected and the concentration of lactate dehydrogenase (LDH) was measured using an LDH test kit from Nanjing Jiancheng Bioengineering Institute, China. The results were obtained using a spectrophotometer with a light path of 1 cm at a wavelength of 440 nm.

TEM examination of cell pyroptosis

Following the digestion of the cell samples with trypsin and subsequent centrifugation, they were allowed to remain at room temperature for 1 h. Subsequently, they were stored at a temperature of 4 °C until 12 h before to their submission for evaluation. After replacing the fixative with a PBS solution, the samples were sent for testing. The Center Laboratory of Southern Medical University processed these samples and viewed and photographed them using a Hitachi H-7500 transmission electron microscope.

Cryopreservation and Cryosectioning

Tissue samples are quickly frozen and immersed in cryoprotectant to solidify, then sliced into thin sections with a cryostat. The sections are placed on slides for DAPI staining, and fluorescence is observed using a confocal microscope.

In vivo toxicity assessment: hematological analysis and histology

For the purpose of assessing toxicity in living organisms, evaluations were performed on day 28 following the last injection. AST (aspartate aminotransferase), ALT (alanine aminotransferase), BUN (blood urea nitrogen), and creatinine levels were determined using commercially available assay kits obtained from Nanjing Jiancheng Bioengineering Institute, China. Tissue samples from many organs (including the heart, liver, spleen, lung, kidney, and uterine) were obtained 28 days after the final injection. The samples were conserved in a solution of containing 4% paraformaldehyde, thereafter encased in paraffin, sectioned into 5 μm slices, and stained with H&E for histological analysis.

Statistical Analysis

Data analysis was performed using SPSS Statistics 20 and GraphPad Prism 9.0.0. Average values and standard deviations (SD) were reported. The Student's t-test was used to compare two groups, while one-way analysis of variance (ANOVA) was applied for multiple groups. For normally distributed data, the least significant difference (LSD) method was used; for non-normally distributed data, Dunnett's T3 test was utilized. Statistical significance was defined as a *P*-value of less than 0.05. Each experiment was independently replicated at least three times.

Results

The restorative effect of miR-21 on cisplatin-induced damage in granulosa cells

After introducing lentiviral vectors carrying miR-21, the exogenous miR-21 gene was successfully expressed in KGN cells, demonstrating its restorative effects on cisplatin-induced damage in granulosa cells.

Cell proliferation in KGN cells was assessed using CCK-8 assays at four different time points. The results showed a significant increase in cell

proliferation in the LV-miR-21 + CDDP group compared to the LV-NC + CDDP group, indicating a potential beneficial effect of miR-21 on cell growth (Fig. 1A). Flow cytometry analysis revealed an apoptosis rate of approximately 5% in the LV-NC group, 24% in the LV-NC + CDDP group, 5% in the LV-miR-21 group, and 17% in the LV-miR-21 + CDDP group. The lower apoptosis rate in the LV-miR-21 + CDDP group, relative to the LV-NC + CDDP group, suggests that miR-21 may mitigate cisplatin-induced apoptosis in granulosa cells (Fig. 1B).

Moreover, the levels of E_2 in the culture medium were significantly higher in the LV-miR-21 + CDDP group compared to the LV-NC + CDDP group, as determined by ELISA (Fig. 1C). qRT-PCR results indicated a substantial increase in the expression of genes associated with hormone production in the LV-miR-21 + CDDP group compared to the LV-NC + CDDP group (Fig. 1D). Western blot analysis revealed a significant reduction in the protein levels of pyroptosis-related genes in the LV-miR-21 + CDDP group (Fig. 1E). Additionally, mRNA expression levels of these pyroptosis-related genes were significantly lower in the LV-miR-21 + CDDP group than in the LV-NC + CDDP group (Fig. 1F).

Extraction and identification of miR-21-Exo

After transfection with lentiviral vectors encoding miR-21, the exogenous miR-21 gene had been effectively expressed in BMSC. The gradient ultracentrifugation technique was employed to isolate Exo utilizing the growth medium of miR-21-BMSC or BMSC. Both the absorbed miR-21-Exo and Exo exhibited a characteristic double-layer membrane structure under transmission electron microscopy (Fig. 2A). The proteins TSG101, CD81, and CD9 were detected in both miR-21-Exo and Exo samples (Fig. 2B). The mean diameters of miR-21-Exo and Exo were (81.9 ± 18.74) nm and (77.8 ± 15.45) nm, respectively, which are within the accepted range of exosome sizes (50-150 nm) (Fig. 2C). The qRT-PCR analysis revealed a fourfold upregulation in the expression of miR-21 in miR-21-Exo compared to Exo (Fig. 2D).

miR-21-Exo suppressed CDDP-induced pyroptosis in KGN cells and enhanced hormone production

During confocal microscopy observations, KGN cells that were harmed by cisplatin exhibited red fluorescence signals surrounding the nucleus, which indicated their capacity to absorb miR-21-Exo or Exo (Fig. 3A). The CCK8 assay findings demonstrated that miR-21-Exo effectively reduced the prolonged growth suppression caused by cisplatine in KGN cells (Fig. 3B). Additional inquiries carried out to evaluate the effect of miR-21-Exo on the process of cisplatin-induced apoptosis in KGN cells. Annexin V-FITC/PI double labeling and flow cytometry analysis revealed a significant reduction in apoptosis rate in the miR-21-Exo-treated group as compared to the cisplatin-treated group (Fig. 3C). The results suggest that miR-21-Exo has the ability to prevent cisplatin-induced cell death in KGN cells in a laboratory setting. In addition, the assessment of E_2 levels in the liquid surrounding the cell cultures revealed a notable rise in E_2 concentration in the liquid of the CDDP + Exo and CDDP + miR-21-Exo groups, in comparison to the cisplatin group (Fig. 3D). When compared to the cisplatin group, the qRT-PCR results demonstrated that miR-21-Exo substantially enhanced the mRNA expression levels of genes associated to hormone production (FSHR, CYP11A1, CYP19A1, HSD17B1, STAR).

When evaluating the cell culture supernatants, it was seen that the cisplatin group had elevated levels of LDH, indicating damage to the cell membrane. However, the introduction of miR-21-Exo led to reduced LDH levels (Fig. 3F). Electron microscope measurements revealed that cells in the model group displayed both edema and an increase in protrusions. In contrast, cells in the miR-21-Exo group showed decreased protrusions, suggesting that miR-21-Exo may suppress cell pyroptosis (Fig. 3G). Western Blotting tests were conducted to measure the expression levels of pyroptosis-related proteins, including NLRP3, CASP1, and GSDMD. The results showed a notable reduction in protein expression in the CDDP + miR-21-Exo group as compared to the CDDP group (Fig. 3H). Furthermore, qRT-PCR was performed to analyze the expression levels of genes related to pyroptosis, such as NLRP3, CASP1, GSDMD, IL1β, and IL18. The findings indicated a notable reduction in mRNA expression levels in the

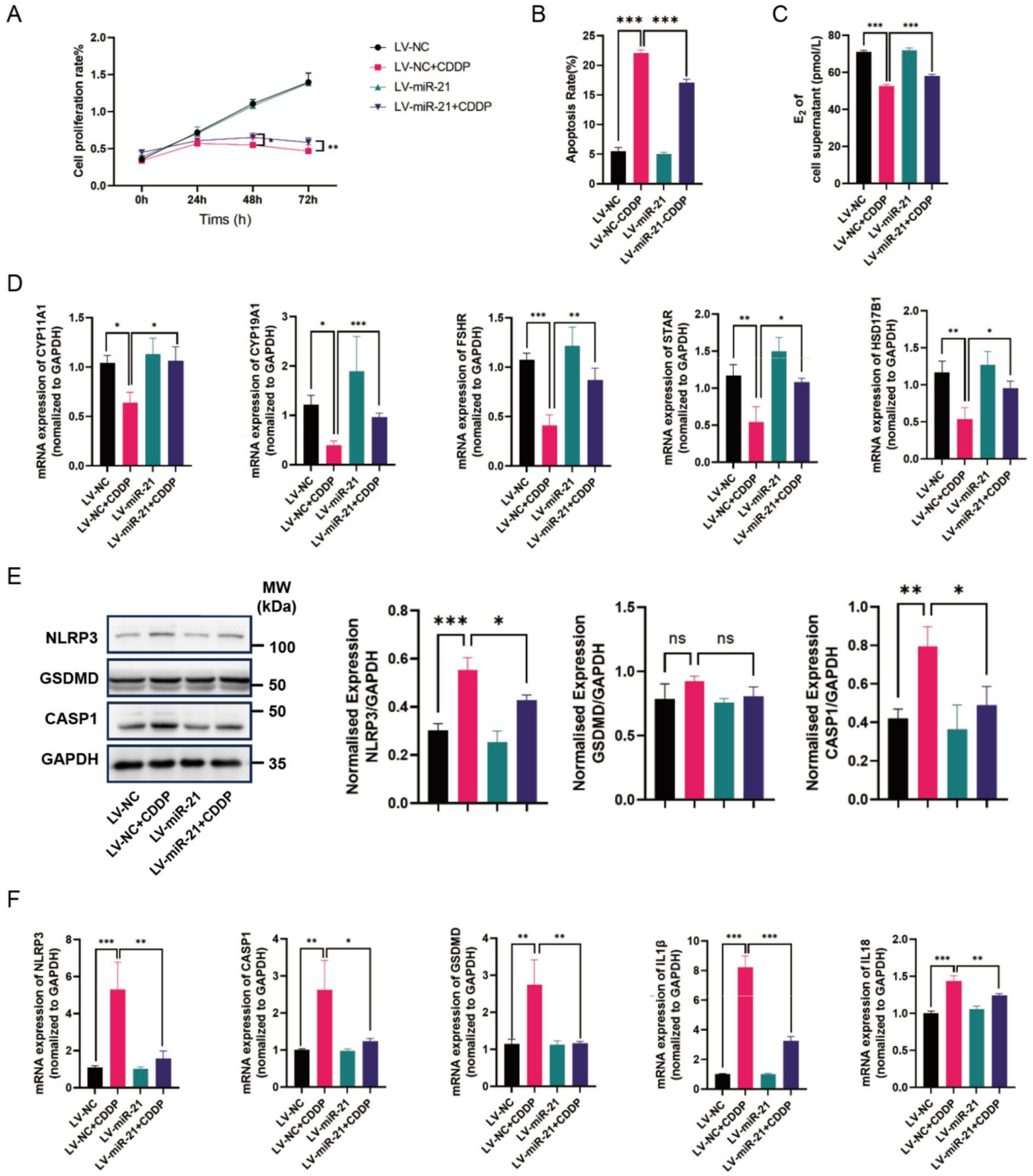

Fig. 1 The restorative effect of miR-21 on cisplatin-induced granulosa cells. (**A**) The CCK8 test (n = 3) was used to determine the proliferation rate. (**B**) The level of apoptosis was assessed using fluorescence-activated cell sorting (n = 3). (**C**) An enzyme-linked immunosorbent assay was used to quantify the levels of E_2 in the cell supernatants (n = 3). (**D**) The mRNA levels of FSHR, CYP11A1, CYP19A1, HSD17B1, and STAR were measured using qRT-PCR and standardized against GAPDH (n = 3). (**E**) The protein levels of pyroptosis-related genes NLRP3, CASP1, and GSDMD were measured using Western Blotting and analyzed using ImageJ software (n = 3). (**F**) The mRNA levels of NLRP3, CASP1, GSDMD, IL1β, and IL18 were measured using qRT-PCR and standardized against GAPDH (n = 3)

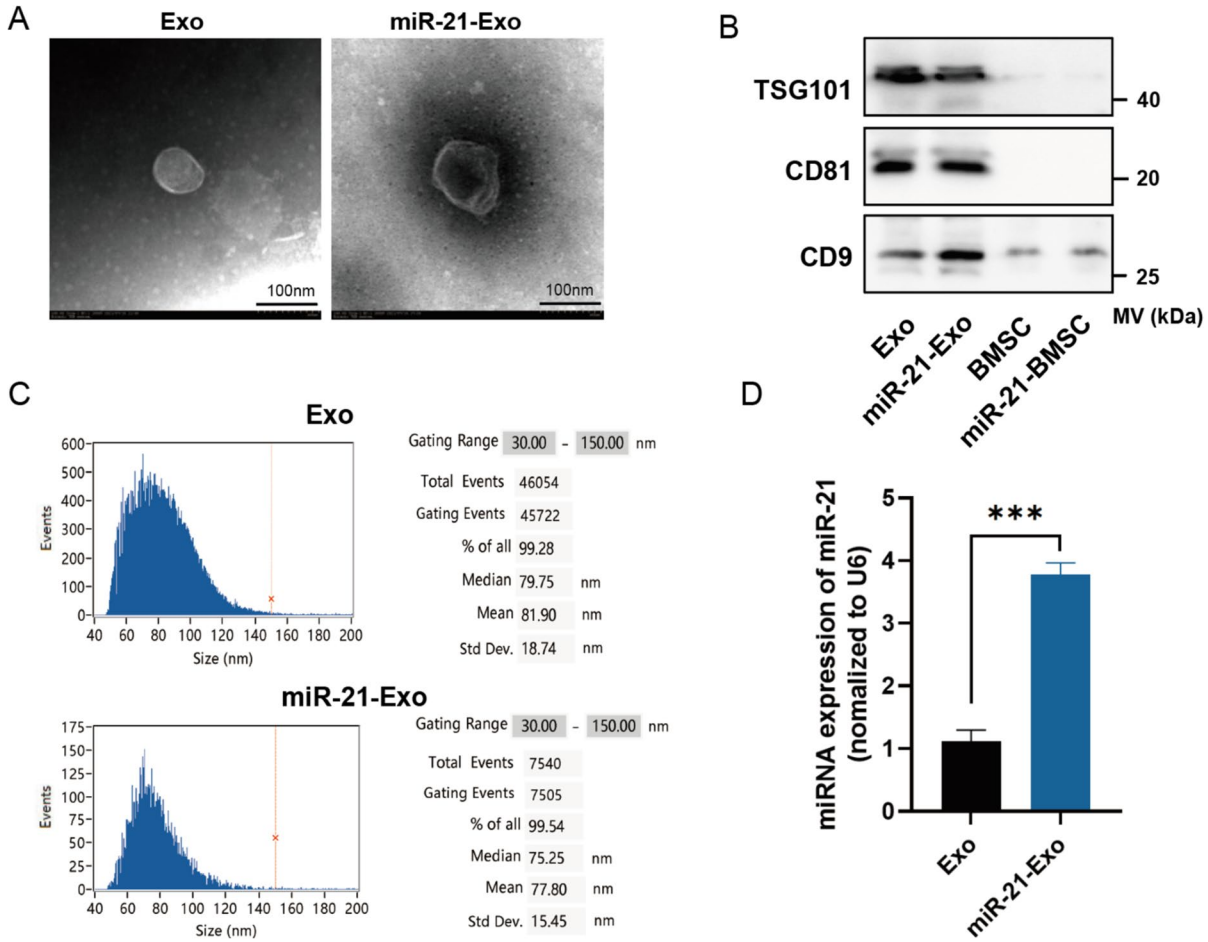

Fig. 2 Extraction and identification of miR-21-Exo. (**A**) Transmission electron microscopy (n = 3) was utilized to investigate the structure of Exo and miR-21-Exo. (**B**) Exo and miR-21-Exo (n = 3) were analyzed with a Flow NanoAnalyzer to assess their particle sizes. (**C**) TSG101, CD81, and CD9 membrane protein levels in Exo and miR-21-Exo samples (n = 3) were measured. (**D**) The expression level of the miR-21 gene was assessed in BMSC and in Exo generated from BMSC transfected with miR-21 (n = 3). Standardization of the expression levels to U6 was done

CDDP + miR-21-Exo group when compared to the cisplatin group (Fig. 3I).

miR-21-Exo regulated the MALT1 and NF-κB signaling pathways

We utilized five widely used miRNA target gene prediction platforms, namely Tarbase, miRDB, DIANA tools, miRTarBase, and miRWalk, to forecast the potential target genes of miR-21. The intersection of the potential target genes with genes closely associated with pyroptosis did not produce any overlapping results. However, when the potential target genes were intersected with the NF-κB signaling pathway, which is known to be connected with pyroptosis, the target gene MALT1, which is associated with pyroptosis, was identified (Fig. 4A). This discovery indicates that miR-21 may play a role in controlling pyroptosis by affecting the expression of MALT1.

To validate the regulatory role of miR-21 on the expression of MALT1 in KGN cells, we utilized lentivirus containing miR-21 to introduce it into KGN cells. We then applied qRT-PCR to assess the influence of miR-21 on the mRNA level of MALT1 in KGN cells. The findings demonstrated that the increased production of miR-21 in KGN cells caused a notable reduction in the levels of MALT1 mRNA expression, regardless of the induction of cisplatin.

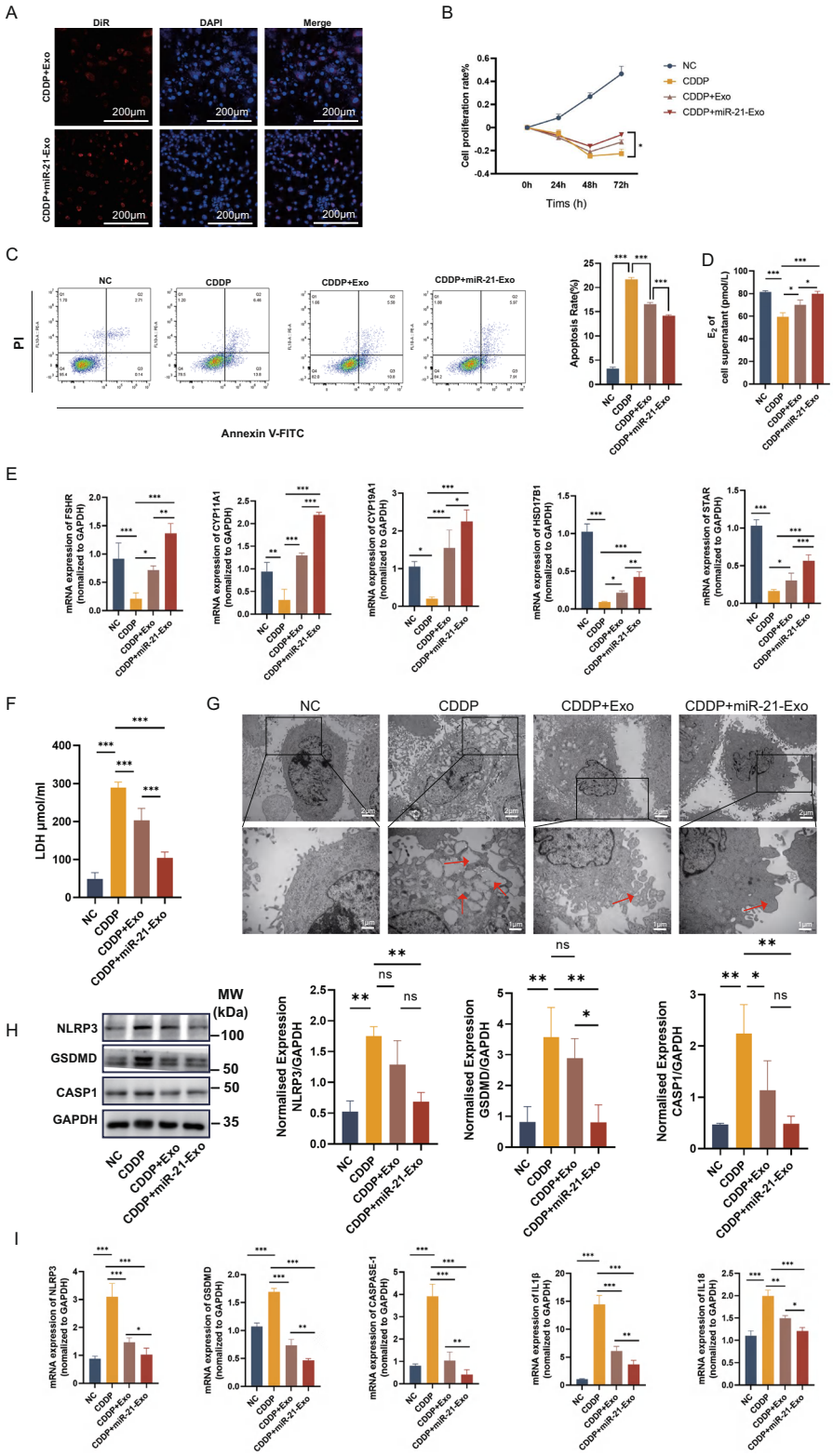

Fig. 3 miR-21-Exo enhanced the activity of CDDP-treated KGN cells. (**A**) CDDP-induced KGN cells (n = 3) were employed to observe the absorption of DiR-labeled Exo or miR-21-Exo using confocal microscopy. (**B**) Using the CCK8 test to calculate the proliferation rate (n = 3). (**C**) Using fluorescence-activated cell sorting to determine the rate of apoptosis (n = 3). (**D**) Measurement of estradiol concentration in cell supernatants using ELISA (n = 3). (**E**) qRT-PCR analysis (n = 3) of the mRNA levels of FSHR, CYP11A1, CYP19A1, HSD17B1, and STAR1, and normalized to GAPDH. (**F**) Quantification of LDH content in cell supernatants (n = 3). (**G**) Observation of cell morphology under electron microscopy. (**H**) Using Western Blotting and ImageJ software, the protein expressions of the pyroptosis-related genes NLRP3, CASP1, and GSDMD were analyzed (n = 3). (**I**) Using qRT-PCR (n = 3) and normalization to GAPDH, the mRNA levels of NLRP3, CASP1, GSDMD, IL1β, and IL18 were determined

This confirms the regulatory function of miR-21 on MALT1 mRNA expression. Furthermore, the level of MALT1 mRNA was considerably elevated in cisplatin-induced KGN cells. Both the group administered with CDDP + Exo and the group administered with CDDP + miR-21-Exo showed a reduction in MALT1 mRNA expression relative to the control group. In the experiment where miR-21 mimic was introduced into 293 T cells, both the miR-21-mimic group and the miR-21-mimetic + CDDP group exhibited decreased MALT1 mRNA expression, thereby validating the regulatory influence of miR-21 on MALT1 (Fig. 4B).

The predictions derived from the miRDB database indicate that miR-21 exhibits a distinct affinity for the mRNA 3'UTR region of MALT1. Consequently, MALT1 has been chosen as a primary target for further investigation (Fig. 4C).

In addition, the findings from the dual-luciferase reporter experiments provided evidence that miR-21 has the ability to selectively target MALT1 and suppress the production of its mRNA (Fig. 4D). The protein expression levels of genes implicated in the NF-κB signaling pathway were analyzed by Western Blotting. The results revealed a decrease in the expression levels of NF-κB pathway molecules, indicating that miR-21 may impact the NF-κB signaling pathway by controlling MALT1, which is strongly associated with the regulation of pyroptosis (Fig. 4E).

The increase of MALT1 suppressed the activity of miR-21-Exo

Utilizing the MALT1-OE vector from IGE Biotechnology in China, the possibility of the miR-21/MALT1/NF-κB signaling pathway playing a role in the pyroptosis process was investigated. Initially, the cells were genetically modified using the MALT1 plasmid, and then cisplatin (CDDP) was added as the starting time point (0-h). Compared to the CDDP + miR-21-Exo group, the results show a significant decrease in cell proliferation in the CDDP + miR-21-Exo + OE-MALT1 group. This suggests that MALT1 has a suppressive function in the proliferation of KGN cells (Fig. 5A). The flow cytometry investigation revealed a significantly elevated rate of apoptosis in the CDDP + miR-21-Exo + OE-MALT1 group compared to the CDDP + miR-21-Exo group (Fig. 5B). When the E_2 content in the liquid surrounding the cell culture was quantified, it was found that the CDDP + miR-21-Exo + OE-MALT1 group had much less E_2 than the CDDP + miR-21-Exo group (Fig. 5C). In addition, the qRT-PCR analysis of mRNA expression levels of different enzymes implicated in cell hormone synthesis showed a decrease in the expression of FSHR, CYP11A1, CYP19A1, HSD17B1, and STAR in the CDDP + miR-21-Exo + OE-MALT1 group compared to the CDDP + miR-21-Exo group. These differences were statistically significant (Fig. 5D). The protective effect of miR-21-Exo against cisplatin-induced granulosa cell hormone synthesis is attenuated when MALT1 is overexpressed. The expression of genes related to pyroptosis, both at the protein and mRNA levels, demonstrated an upward trajectory. Additionally, there was a notable rise in the expression of proteins associated with the NF-κB signaling pathway. Consequently, this counteracted the suppressive impact of miR-21-Exo on pyroptosis and the NF-κB signaling pathway (Fig. 5E, F, G).

miR-21-Exo restored the estrous cycle and hormones in chemically-induced ovarian insufficiency rats

To create an in vivo model of chemotherapy-induced ovarian insufficiency, SD rats received intraperitoneal injections of CDDP at a dose of 1 mg/kg for 14 consecutive days. After this treatment, the rats were administered either miR-21-Exo or Exo, while the control group was injected with PBS. Rats from each group were euthanized at different time points to assess molecular, histological, and reproductive function (Fig. 6A).

Following the intraperitoneal injection of DiR-labeled miR-21-Exo or Exo into the ovaries, one rat was randomly selected for live imaging. The fluorescence intensity peaked within one hour post-injection, gradually declining to lower levels by 48 h. Imaging at 21 and 28 days also revealed a significant reduction in fluorescence intensity (Fig. 6B). Confocal microscopy confirmed the presence of red fluorescence from DiR-labeled miR-21-Exo or Exo in ovarian tissues, following DAPI labeling of frozen sections, validating the effective uptake by the ovaries and the feasibility of the injection method (Fig. 6C).

Vaginal cytology smears were analyzed to track changes in the estrous cycle, showing that the POI group experienced disrupted cycles with reduced frequency. In contrast, the groups treated with

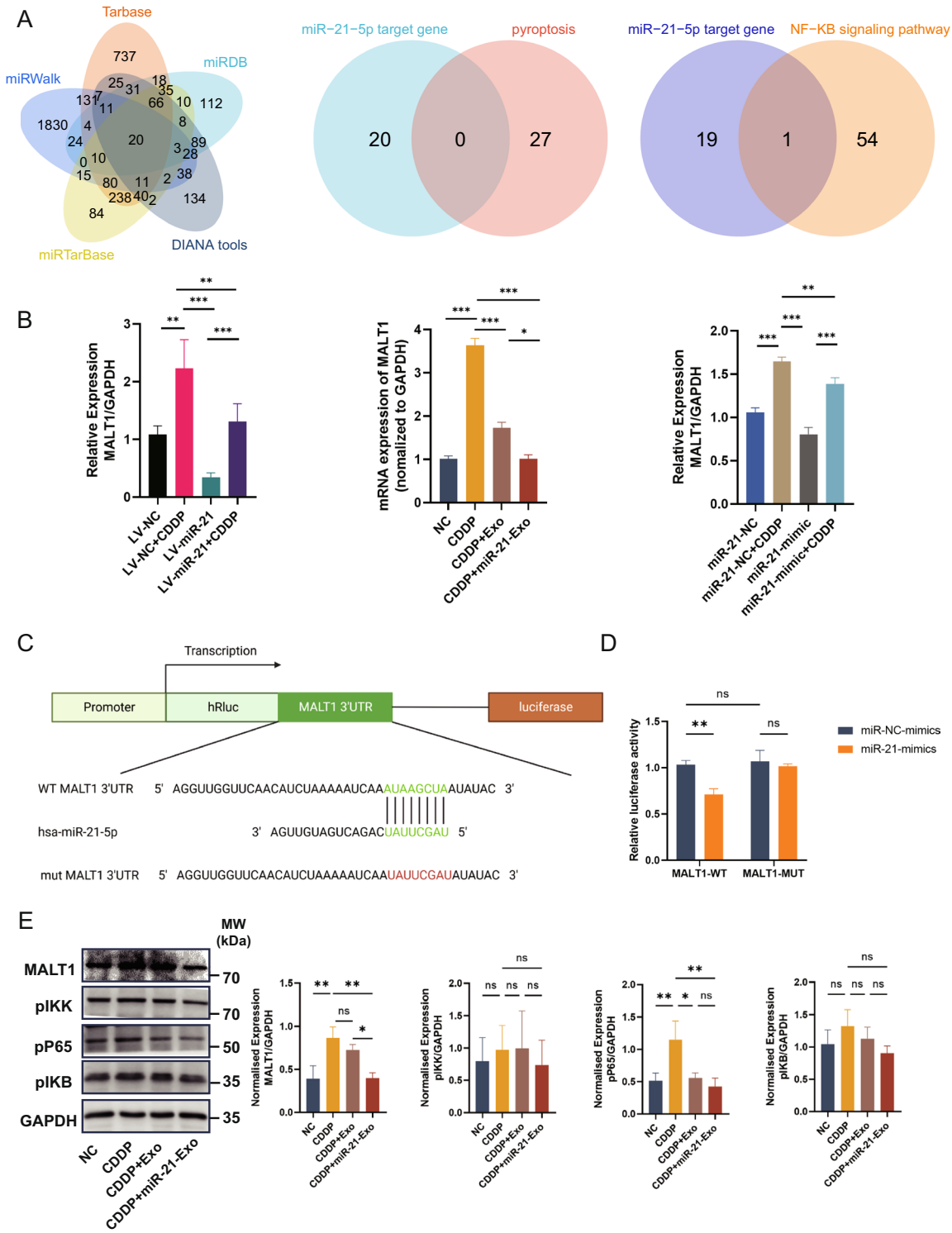

miR-21-Exo or Exo exhibited significant improvement in estrous cycle regularity, indicated by an increased number of estrous phases (Fig. 6D). Hormonal assessments in blood samples collected at various intervals showed that compared to the POI group, the miR-21-Exo or Exo treatment group had

◂**Fig. 4** miR-21-Exo regulated the MALT1 and NF-κB signaling pathways. (**A**) P The identification of pyroptosis-related MALT1 as a putative target gene of miR-21 via intersection (Data Sources: Tarbase, miRDB, DIANA tools, miRTarBase, miRWalk, rectome and GeneCards). (**B**) The expression of MALT1 mRNA is regulated by miR-21 (n = 3). (**C**) miRDB database predicts the specific binding site of miR-21 with MALT1 (n = 3). (**D**) Results from dual-luciferase reporter assays demonstrate the specific targeting of MALT1 by miR-21 (n = 3). The sequence's altered portion is denoted as MALT1-MUT. MALT1-WT denotes the wild-type MALT1 (n = 3). (**E**) Validation of the impact of miR-21 on the protein expression levels of the NF-κB signaling pathway through Western Blotting (n = 3)

significantly elevated E_2 levels, reduced FSH levels, and a notable increase in AMH levels (Fig. 6E).

miR-21-Exo repaired the structure of the rats ovaries, improved reproductive function, promoted proliferation, and inhibited apoptosis

After performing surgery to extract the ovaries and separate the surrounding fat pads from sedated rats, bilateral ovaries were collected. Macroscopic examination revealed that the ovaries of POI rats were smaller, had a uniform appearance, and lacked noticeable follicles. In contrast, rats injected with miR-21-Exo or Exo showed a significant increase in ovarian volume and the presence of follicle-like structures on the surface (Fig. 7A).

Following slicing and HE staining of the ovarian tissues, scans revealed that the POI ovaries had a reduced volume and a lower count of mature follicles (Fig. 7B). To assess the impact of miR-21-Exo or Exo on reproductive function, paired experiments were conducted, with observations made after ten days of cohabitation. The results indicated a low pregnancy rate in the POI group, while the miR-21-Exo and Exo groups had significantly higher pregnancy rates. Notably, the miR-21-Exo group produced more offspring than the Exo group (Fig. 7C).

Further analysis of the follicles showed a significant decrease across all stages in the POI group. Conversely, injection of miR-21-Exo or Exo resulted in a substantial increase in follicle numbers at all stages, without affecting the count of secondary follicles (Fig. 7D). Intraperitoneal administration of miR-21-Exo or Exo preserved follicle counts in POI rats.

Immunohistochemical analysis of PCNA expression in granulosa cells indicated a marked reduction in the POI group compared to the control group. However, PCNA levels in the miR-21-Exo and Exo treatment groups were significantly elevated compared to the POI group (Fig. 7E). The TUNEL assay was utilized to detect cell apoptosis in ovarian tissues, and average fluorescence intensity was analyzed using imaging software. The results showed that average fluorescence intensity in the POI group was significantly higher than in the control group. In contrast, both miR-21-Exo and Exo treatment groups exhibited a notable reduction in average fluorescence intensity compared to the POI group, as confirmed by statistical analysis (Fig. 7F).

miR-21-Exo inhibited ovarian pyroptosis in chemotherapy-induced POI rats

In order to examine the pyroptosis condition in ovarian tissues, we performed Western blot tests. The findings demonstrated that the expression of NLRP3, CASP1, and GSDMD pyroptosis-related proteins were reduced in the POI + miR-21-Exo group compared to the POI group (Fig. 8A). Following that, we utilized qRT-PCR to measure the mRNA levels of genes associated with pyroptosis in rat ovarian tissues. The research findings indicated a significant upregulation of the levels of pyroptosis-related genes in the POI group considerably increased compared to the control group. In contrast, the miR-21-Exo group demonstrated a large reduction in the expression of these genes. These differences were statistically significant (Fig. 8A). The presence of NLRP3 and GSDMD proteins in the ovaries of each group of rats was detected as brown-yellow granules. The purpose of these granules was to evaluate the impact of miR-21-Exo on granulosa cells pyroptosis. The results showed an elevation in the levels of NLRP3 and GSDMD proteins in the group with POI, while a reduction was detected in the group treated with miR-21-Exo (Fig. 8C). These findings indicate that in granulosa cells of rats with chemotherapy-induced POI, miR-21-Exo inhibited pyroptosis. These findings suggest that miR-21-Exo can prevent the occurrence of granulosa pyroptosis in living organisms by decreasing the MALT1/NF-κB signaling pathway.

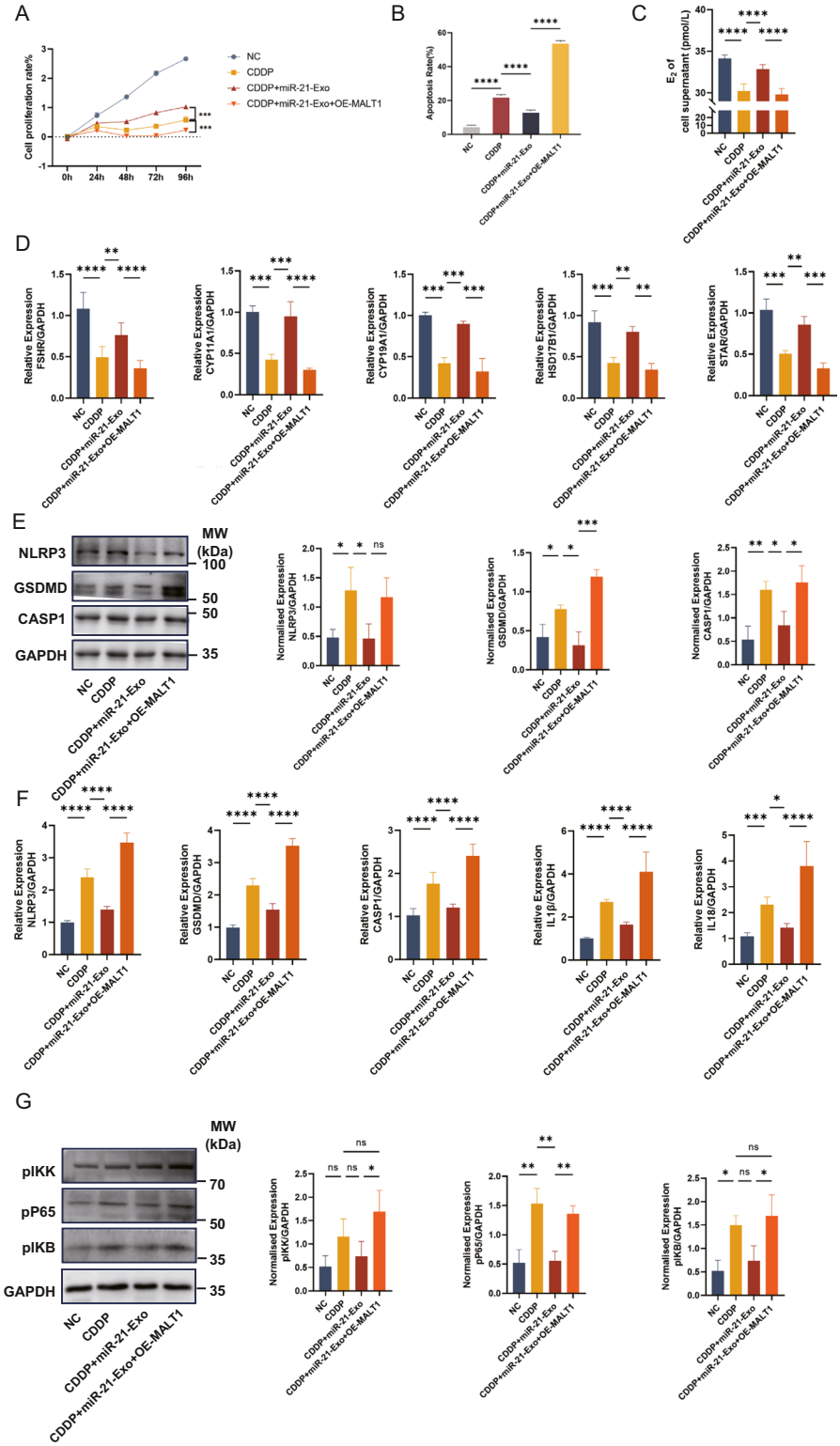

Fig. 5 The increase of MALT1 suppressed the activity of miR-21-Exo. (**A**) Determination of proliferation rate using CCK8 test (n = 3). (**B**) Flow cytometry was used to determine the rate of apoptosis (n = 3). (**C**) Estradiol concentration in cell supernatants was measured using ELISA (n = 3). (**D**) Using qRT-PCR (n = 3), the mRNA levels of FSHR, CYP11A1, CYP19A1, HSD17B1, and STAR1 were determined and normalized against GAPDH. (**E**) Using Western Blotting and ImageJ software, the protein expressions of the pyroptosis-related genes NLRP3, CASP1, and GSDMD were analyzed (n = 3). (**F**) Using qRT-PCR (n = 3) and normalization to GAPDH, the mRNA levels of NLRP3, CASP1, GSDMD, IL1β, and IL18 were determined. (**G**) Using ImageJ software and Western Blotting, the NF-κB signaling pathway's protein expressions were analyzed (n = 3)

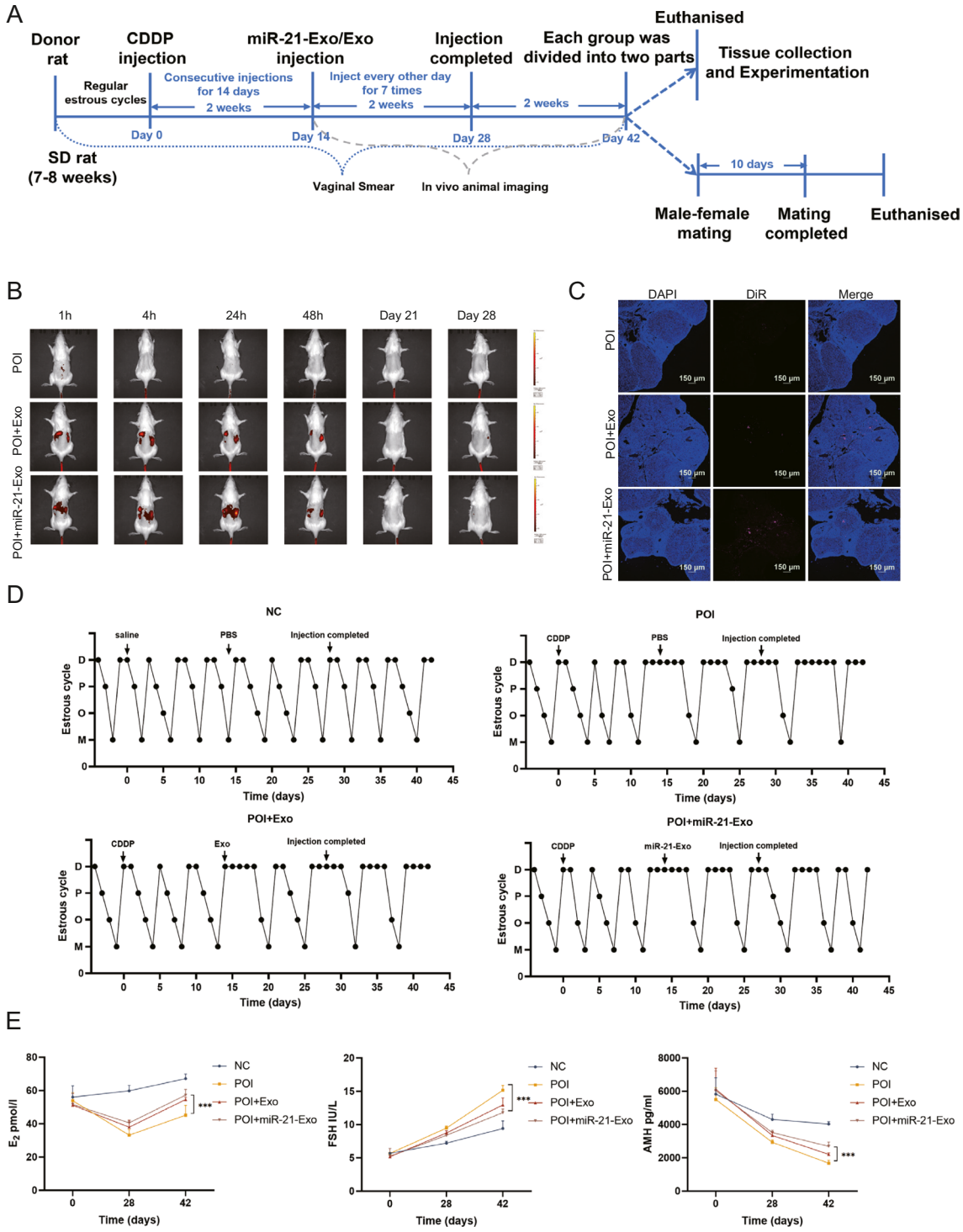

Fig. 6 miR-21-Exo restored the estrous cycle and hormones in chemically-induced ovarian insufficiency rats. (**A**) Schematic schematic illustrating the animal experimental design. (**B**) Intraperitoneal injection of DiR-labeled Exo or miR-21-Exo resulted in in vivo metabolism observed through live animal imaging. (**C**) Ovarian frozen sections showed uptake of DiR fluorescently labeled exosomes by the ovaries. (**D**) Representative estrous cycles of rats exhibiting either regular or interrupted estrous cycles within each group. (**E**) The levels of serum sex hormones E_2, FSH, and AMH were measured using ELISA (n = 4)

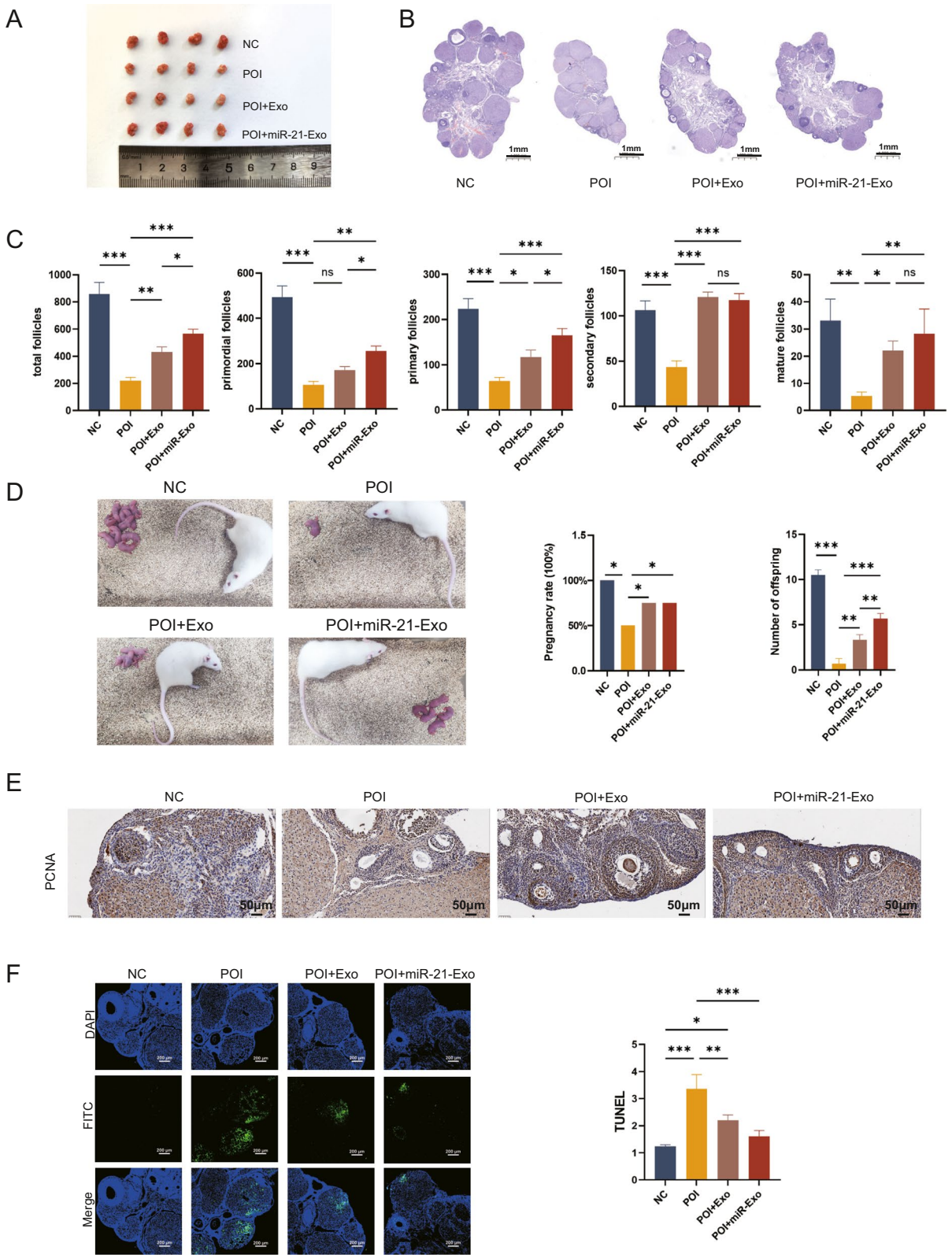
A
NC
POI
POI+Exo
POI+miR-21-Exo
B
1mm
NC
POI
POI+Exo
POI+miR-21-Exo
C
total follicles
primordial follicles
primary follicles
secondary follicles
mature follicles
ns
D
NC
POI
POI+Exo
POI+miR-21-Exo
Pregnancy rate (100%)
Number of offspring
E
PCNA
50μm
F
DAPI
FITC
Merge
TUNEL

◂**Fig. 7** miR-21-Exo repaired the structure of the rats ovaries, improved reproductive function, promoted proliferation, and inhibited apoptosis. (**A**) Macroscopic observation of ovaries in each group (**B**) HE staining of ovarian tissues. (**C**) The number of follicles per ovary was determined in rats (n = 4). (**D**) Litter position diagrams, pregnancy rate, and offspring count in each group (n = 4). (**E**) Immunohistochemistry was used to evaluate the expression of PCNA protein (n = 4). (**F**) The apoptosis of granulosa cells was evaluated using TUNEL labeling (n = 4)

The application of exosomes did not affect the structure and function of major organs in rats

To determine the safety of miR-21-Exo or Exo therapy, we conducted HE staining on the hearts, livers, spleens, lungs, kidneys, and uteruses of isolated rats. The HE staining results indicated that the organ staining in the miR-21-Exo or Exo groups was similar to that of the POI group, with no significant tissue inflammation observed. Additionally, we assessed liver and kidney function by measuring markers such as creatinine, blood urea nitrogen, ALT, and AST. The results indicated no significant increases in these values in the miR-21-Exo or Exo treatment groups. Therefore, miR-21-Exo or Exo demonstrated good biocompatibility and may be considered a promising therapeutic option for rats with chemotherapy-induced early ovarian insufficiency Fig. 9.

Discussion

Chemotherapy-induced premature ovarian insufficiency (POI) can have significant and long-lasting effects on patients' health (Mauri et al. 2020). Therefore, it is essential to identify effective strategies for managing this condition. One study has shown that using BMSC that overexpress miR-21 may help restore ovarian function in individuals with POI, suggesting that miR-21 plays a role in promoting ovarian recovery and protection. (Yin et al. 2024). Additionally, research indicates that miR-21-Exo can aid in restoring autoimmune POI, highlighting their potential as a therapeutic tool for repairing ovarian damage caused by autoimmune conditions (Yang et al. 2024). Exosomes are crucial for cell communication and offer numerous advantages, including high biocompatibility, low immunogenicity, and safety in biological systems (Zhuang et al. 2022). They also have the capacity to transport therapeutic molecules like miR-21 effectively. The findings of this study suggest that miR-21-Exo can significantly enhance the restoration and protection of ovarian function, offering a promising and innovative approach to address chemotherapy-induced POI.

Pyroptosis is an important mechanism of cell death that plays a crucial role in POI. It is a regulated and systematic process that eliminates compromised or damaged cells (Rao et al. 2022). Chemotherapy medications, immunological damage, and oxidative stress can cause pyroptosis in ovarian tissue (Xie et al. 2024; Chen et al. 2023, 2022; Liu et al. 2024; Miao et al. 2023). These factors can initiate the pyroptosis program in cells via various signaling pathways, resulting in cell death and functional impairment of ovarian cells. Research has demonstrated that chemotherapeutic medications can trigger pyroptosis of ovarian cells, leading to diminished ovarian function, decreased follicle counts, and the onset of POI (Miao et al. 2023). Several research have investigated the impact of pyroptosis on POI and have sought to manage POI by manipulating the signaling pathways associated with pyroptosis. For instance, researchers have investigated the potential of certain antioxidants and anti-inflammatory medications to mitigate ovarian cell pyroptosis, therefore safeguarding ovarian function (Liu et al. 2024). Furthermore, scientific investigations have examined advanced techniques including stem cell transplantation and growth factor therapy as means to enhance the restoration and renewal of ovarian tissue, hence mitigating the pathological alterations associated with POI (Ma et al. 2024). Developing innovative strategies to prevent and treat POI by manipulating pyroptosis is crucial for improving the quality of life for POI patients and offers valuable insights for preserving ovarian function.

Initially, a stable expression system was established by transfecting KGN cells with lentivirus carrying miR-21. Afterwards, we treated both KGN cells transfected with an empty vector and KGN cells overexpressing miR-21 with cisplatin or left them untreated. The purpose was to investigate the impact of miR-21 on the repair process induced by cisplatin in KGN cells, focusing on parameters such as cell proliferation, apoptosis, pyroptosis, and sex hormone synthesis. To validate the functionality of miR-21-Exo, BMSC genetically modified by introducing a lentivirus containing miR-21. This resulted in the creation of stable miR-21-BMSC.

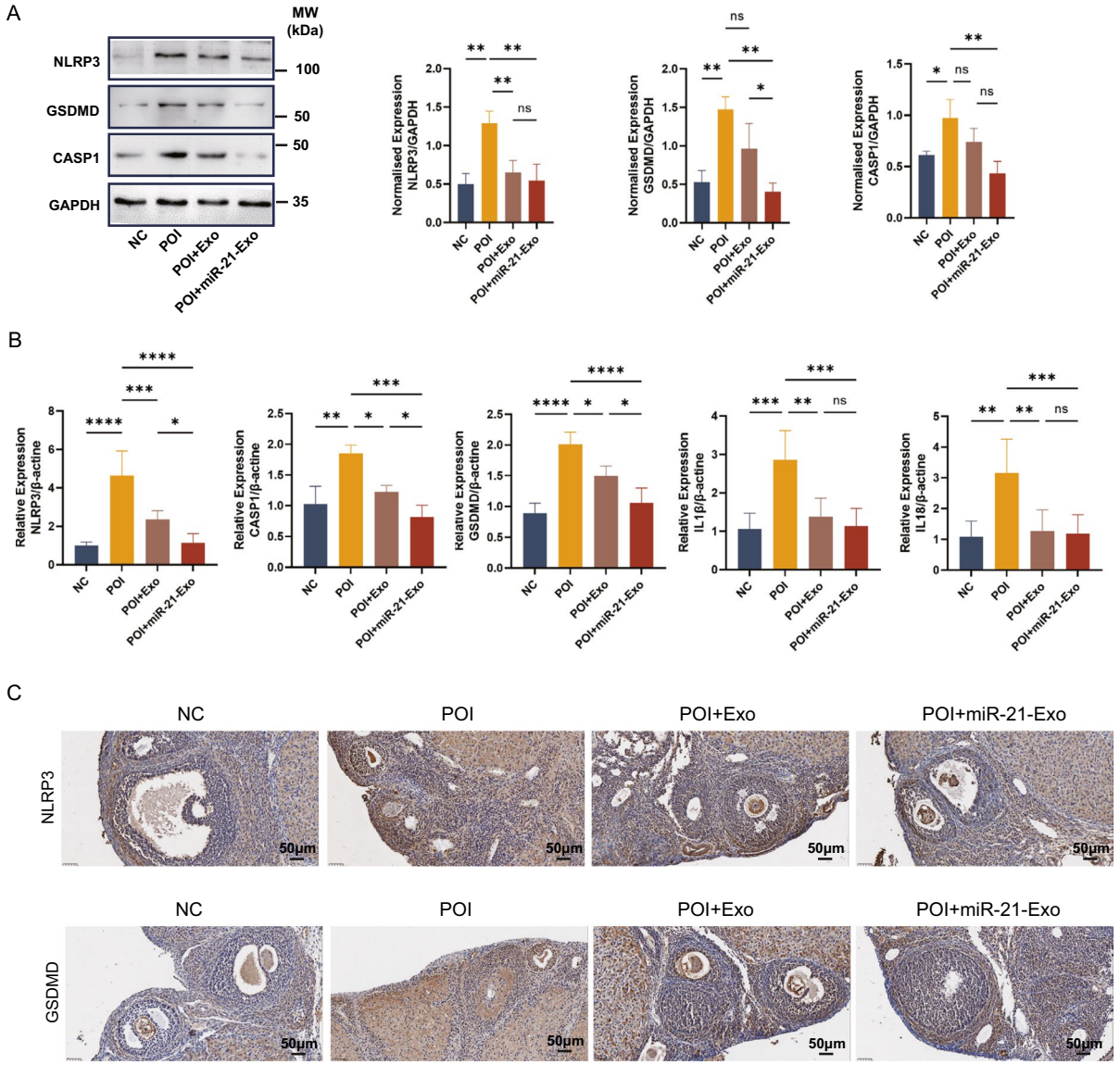

Fig. 8 miR-21-Exo inhibited ovarian pyroptosis in chemotherapy-induced POI rats. (**A**) Western blot analysis was used to determine the expression levels of NLRP3, CASP1, and GSDMD proteins. (**B**) mRNA levels of NLRP3, CASP1, GSDMD, IL1β, and IL18 in the miR-21-Exo group were analyzed by qRT-PCR. (**C**) Immunohistochemical staining was performed for NLRP3 and GSDMD in the ovaries

Subsequently, miR-21-Exo was effectively extracted from these cells using ultracentrifugation. Further validation confirmed the absorption of miR-21-Exo by KGN cells exposed with CDDP and chemotherapy-induced POI rats. This was verified using DiR dye labeling, assessing cellular uptake through confocal microscopy, and analyzing ovarian tissue uptake through frozen section analysis. Notably, miR-21-Exo was found to promote granulosa cell growth, inhibit apoptosis and pyroptosis, and enhance sex hormone production, thereby facilitating recovery from chemotherapy-induced POI both in vitro and in vivo. Bioinformatics analysis identified the downstream target gene MALT1. A dual-luciferase reporter assay confirmed the direct interaction between miR-21 and MALT1, highlighting

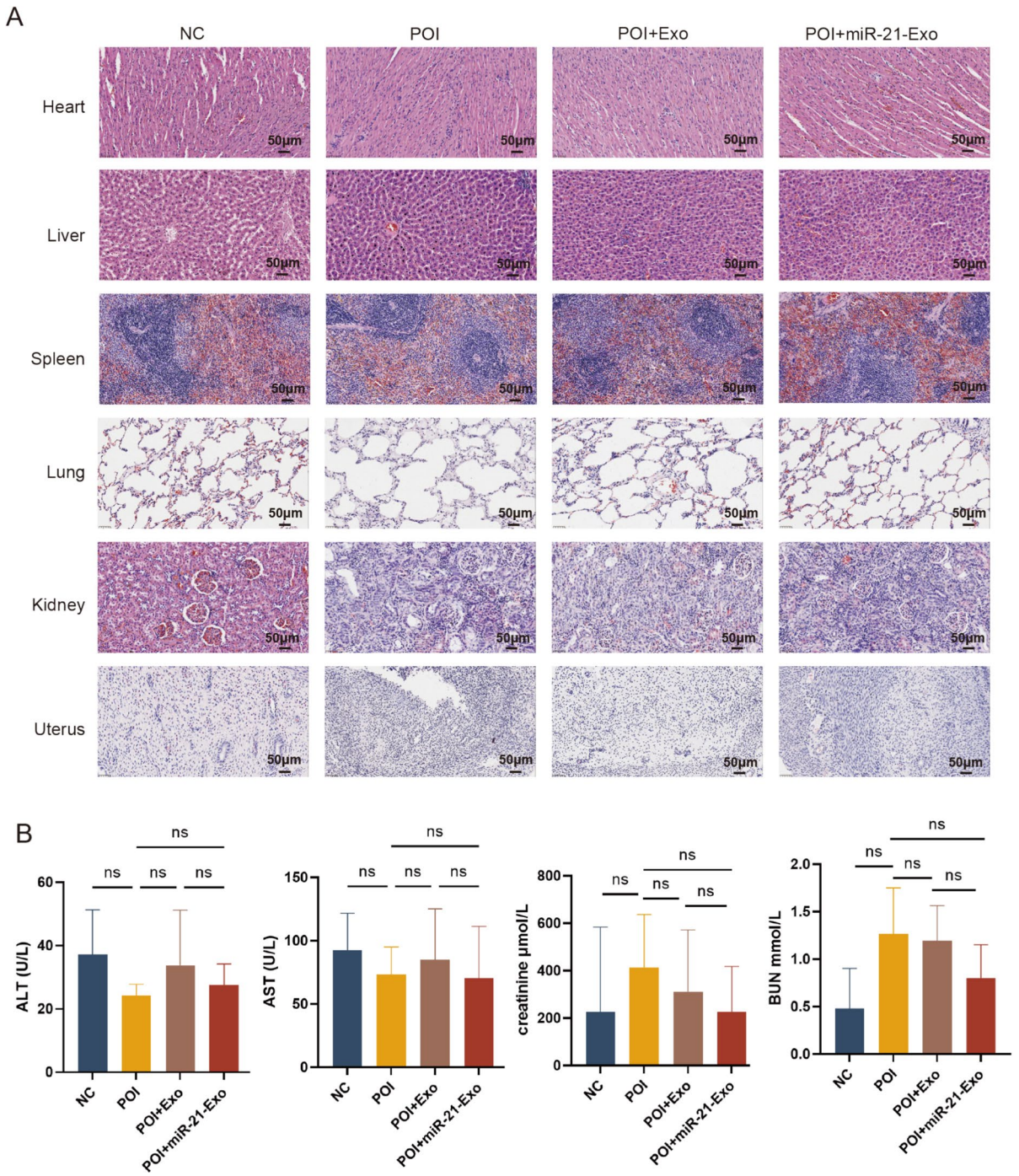

Fig. 9 The application of exosomes did not affect the structure and function of major organs in rats. (**A**) HE diagram of paraffin sections of each organ in each group. (**B**) Detection of liver and kidney function in each group

the role of miR-21 in regulating pyroptosis in granulosa cells through MALT1 modulation.

miR-21 is a significant regulatory microRNA that has a critical role in controlling cell growth, programmed cell death, and metabolic processes (Malvandi et al. 2022; Jenike and Halushka 2021; Surina et al. 2021). Exosomes from BMSC carrying components such as miR-21 have the ability to control the biological functions of granulosa cells in the ovary that have been damaged by chemotherapy. miRNAs carry out their biological functions by repressing the expression of target gene mRNAs (Obernosterer et al. 2006). MALT1 is an essential protein involved in transmitting signals that are critical for regulating immunological responses, cell death, and inflammatory reactions (Wang et al. 2023). The stimulation of the NF-κB signaling pathway can result in the production of inflammatory factors and worsen inflammatory responses, which in turn initiates the process of pyroptosis (Tao et al. 2021; Luo et al. 2022; Zheng et al. 2020). MALT1 is closely associated with the NF-κB pathway and acts as a key regulatory factor in the stimulation of the NF-κB signaling pathway (Fung et al. 2021; Minderman et al. 2023). Research indicates that miR-21 hinders the production of MALT1 by attaching to its 3'UTR, thus suppressing pyroptosis in granulosa cells. This mechanism may elucidate how miR-21 facilitates the repair of cisplatin-induced damage in these cells.

This study demonstrates that miR-21 inhibits apoptosis and pyroptosis in granulosa cells while promoting hormone production. miR-21-Exo can be delivered to the ovary and repair chemotherapy-induced POI by suppressing pyroptosis. Crucially, miR-21-Exo hinder the procedure of granulosa cell pyroptosis by controlling the NF-κB signaling pathway through MALT1. To confirm the therapeutic efficacy of miR-21-Exo in reducing pyroptosis and treating chemotherapy-induced POI in rats, various parameters including hormone concentrations, ovarian structure, estrus cycle, reproductive function, as well as levels of pyroptotic mRNA and proteins were examined.

In summary, this study reveals that miR-21-loaded exosomes derived from BMSCs modulate the NF-κB signaling pathway via MALT1, thereby inhibiting pyroptosis in granulosa cells. These findings offer important insights into molecular therapeutic strategies for managing chemotherapy-induced POI. The Graphical Abstract provides a clear overview of this research.

Acknowledgements Not applicable

Authors' contributions L.T. and Y.Y. conducted the experiments and drafted the paper; M.Y. , J. X and Y. Z. coordinated the study; A.Z., Y.W. and M.M. revised the manuscript; X.F. designed the study and revised the paper. The authorship is in the order of contributions. All the authors have read and approved the final manuscript.

Funding This study received funding from the National Natural Science Foundation of China (No. 82271657), the Natural Science Foundation of Guangdong Province (No. 2024A1515010460), and the Guangzhou Municipal Science and Technology Project.

Data availability No datasets were generated or analysed during the current study.

Declarations

Ethics approval and informed consent All animal experiments conducted was compliant with the Ethics Committee of Southern Medical University Zhujiang Hospital (No: LAEC-2022–208).

Consent for publication Not applicable.

Competing interests The authors declare no competing interests.

References

Cai JH, Sun YT, Bao S. Hucmscs-exosomes containing mir-21 promoted estrogen production in ovarian granulosa cells via lats1-mediated phosphorylation of loxl2 and yap. Gen Comp Endocrinol. 2022;321–322:114015. https://doi.org/10.1016/j.ygcen.2022.114015.

Chen D, Hu N, Xing S, Yang L, Zhang F, GuoMa SH. Placental mesenchymal stem cells ameliorate nlrp3 inflammasome-induced ovarian insufficiency by modulating macrophage m2 polarization. J Ovarian Res. 2023;16(1):58. https://doi.org/10.1186/s13048-023-01136-y.

Chen Y, Zhao Y, Miao C, Yang L, Wang R, Chen B, Zhang Q. Quercetin alleviates cyclophosphamide-induced premature ovarian insufficiency in mice by reducing mitochondrial oxidative stress and pyroptosis in granulosa cells. J Ovarian Res. 2022;15(1):138. https://doi.org/10.1186/s13048-022-01080-3.

Ding C, Qian C, Hou S, Lu J, Zou Q, Li H, Huang B. Exosomal mirna-320a is released from hamscs and regulates sirt4 to prevent reactive oxygen species generation in poi. Mol Ther Nucleic Acids. 2020a;21:37–50. https://doi.org/10.1016/j.omtn.2020.05.013.

Ding C, Zhu L, Shen H, Lu J, Zou Q, HuangHuang CB. Exosomal mirna-17-5p derived from human umbilical cord mesenchymal stem cells improves ovarian function in premature ovarian insufficiency by regulating sirt7. Stem Cells. 2020b;38(9):1137–48. https://doi.org/10.1002/stem.3204.

Fung SY, Lu HY, Sharma M, Sharma AA, Saferali A, JiaTurvey ASE. Malt1-dependent cleavage of hoil1 modulates canonical nf-κb signaling and inflammatory responsiveness. Front Immunol. 2021;12:749794. https://doi.org/10.3389/fimmu.2021.749794.

Huang X, Wu B, Chen M, Hong L, Kong P, Wei Z, Teng X. Depletion of exosomal circLDLR in follicle fluid derepresses miR-1294 function and inhibits estradiol production via CYP19A1 in polycystic ovary syndrome. Aging (Albany NY). 2020;12(15):15414–35.

Jenike AE, Halushka MK. Mir-21: a non-specific biomarker of all maladies. Biomark Res. 2021;9(1):18. https://doi.org/10.1186/s40364-021-00272-1.

Liao Z, Liu C, Wang L, Sui C, Zhang H. Therapeutic role of mesenchymal stem cell-derived extracellular vesicles in female reproductive diseases. Front Endocrinol (Lausanne). 2021;12:665645. https://doi.org/10.3389/fendo.2021.665645.

Liu K, Wu Y, Yang W, Li T, Wang Z, XiaoLei SX. A-ketoglutarate improves ovarian reserve function in primary ovarian insufficiency by inhibiting nlrp3-mediated pyroptosis of granulosa cells. Mol Nutr Food Res. 2024;68(5):e2300784. https://doi.org/10.1002/mnfr.202300784.

Luo L, Liu M, Fan Y, Zhang J, Liu L, LiWu YY. Intermittent theta-burst stimulation improves motor function by inhibiting neuronal pyroptosis and regulating microglial polarization via tlr4/nfκb/nlrp3 signaling pathway in cerebral ischemic mice. J Neuroinflammation. 2022;19(1):141. https://doi.org/10.1186/s12974-022-02501-2.

Ma WQ, Zhuo AP, Xiao YL, Gao M, Yang YT, TangFu LCXF. Human bone marrow derived-mesenchymal stem cells treatment for autoimmune premature ovarian insufficiency. Stem Cell Rev Rep. 2024;20(2):538–53. https://doi.org/10.1007/s12015-023-10629-8.

Malvandi AM, Rastegar-Moghaddam SH, Ebrahimzadeh-Bideskan S, Lombardi G, Ebrahimzadeh-Bideskan A, Mohammadipour A. Targeting mir-21 in spinal cord injuries: a game-changer? Mol Med. 2022;28(1):118. https://doi.org/10.1186/s10020-022-00546-w.

Mauri D, Gazouli I, Zarkavelis G, Papadaki A, Mavroeidis L, GkouraKampletsas SE. Chemotherapy associated ovarian failure. Front Endocrinol (Lausanne). 2020;11:572388. https://doi.org/10.3389/fendo.2020.572388.

Meldolesi J. Exosomes and ectosomes in intercellular communication. Curr Biol. 2018;28(8):R435–44. https://doi.org/10.1016/j.cub.2018.01.059.

Miao C, Zhao Y, Chen Y, Wang R, Ren N, ChenZhang BQ. Investigation of he's yang chao recipe against oxidative stress-related mitophagy and pyroptosis to improve ovarian function. Front Endocrinol (Lausanne). 2023;14:1077315. https://doi.org/10.3389/fendo.2023.1077315.

Minderman M, Lantermans HC, Grüneberg LJ, Cillessen S, Bende RJ, van NoeselSpaargaren CM. Malt1-dependent cleavage of cyld promotes nf-κb signaling and growth of aggressive b-cell receptor-dependent lymphomas. Blood Cancer J. 2023;13(1):37. https://doi.org/10.1038/s41408-023-00809-7.

Obernosterer G, Leuschner PJ, Alenius M, Martinez J. Post-Transcriptional Regulation of Microrna Expression Rna. 2006;12(7):1161–7. https://doi.org/10.1261/rna.2322506.

Qu Q, Liu L, Cui Y, Liu H, Yi J, BingBi WY. Mir-126-3p containing exosomes derived from human umbilical cord mesenchymal stem cells promote angiogenesis and attenuate ovarian granulosa cell apoptosis in a preclinical rat model of premature ovarian failure. Stem Cell Res Ther. 2022;13(1):352. https://doi.org/10.1186/s13287-022-03056-y.

Rao Z, Zhu Y, Yang P, Chen Z, Xia Y, QiaoWang CZ. Pyroptosis in inflammatory diseases and cancer. Theranostics. 2022;12(9):4310–29. https://doi.org/10.7150/thno.71086.

Rebar RW. Premature ovarian failure. Obstet Gynecol. 2009;113(6):1355–63. https://doi.org/10.1097/AOG.0b013e3181a66843.

Surina S, Fontanella RA, Scisciola L, Marfella R, Paolisso G, Barbieri M. Mir-21 in human cardiomyopathies. Front Cardiovasc Med. 2021;8:767064. https://doi.org/10.3389/fcvm.2021.767064.

Tao H, Li W, Zhang W, Yang C, Zhang C, LiangGeng XD. Urolithin a suppresses rankl-induced osteoclastogenesis and postmenopausal osteoporosis by, suppresses inflammation and downstream nf-κb activated pyroptosis pathways. Pharmacol Res. 2021;174:105967. https://doi.org/10.1016/j.phrs.2021.105967.

Thabet E, Yusuf A, Abdelmonsif DA, Nabil I, Mourad G, Mehanna RA. Extracellular vesicles mirna-21: a potential therapeutic tool in premature ovarian dysfunction. Mol Hum Reprod. 2020;26(12):906–19. https://doi.org/10.1093/molehr/gaaa068.

Tilly JL. Ovarian follicle counts–not as simple as 1, 2, 3. Reprod Biol Endocrinol. 2003;1:11. https://doi.org/10.1186/1477-7827-1-11.

Tsiligiannis S, Panay N, Stevenson JC. Premature ovarian insufficiency and long-term health consequences. Curr Vasc Pharmacol. 2019;17(6):604–9. https://doi.org/10.2174/1570161117666190122101611.

Wang J, Gan L, Li F, Li Q, Wu T, WuLei ZL. Tracheal epithelial cell-exosome-derived mir-21-5p inhibits alveolar macrophage pyroptosis to resist pulmonary bacterial infection through pik3cd-autophagy pathway. Life Sci. 2024;336:122340. https://doi.org/10.1016/j.lfs.2023.122340.

Wang Y, Liu Z, Zhang M, Yu B, Ai F. Mucosa-associated lymphoid tissue lymphoma translocation protein 1 exaggerates multiple organ injury, inflammation, and immune cell imbalance by activating the nf-κb pathway in sepsis. Front Microbiol. 2023;14:1117285. https://doi.org/10.3389/fmicb.2023.1117285.

Webber L, Davies M, Anderson R, Bartlett J, Braat D, CartwrightVermeulen BN. Eshre guideline: management of women with premature ovarian insufficiency. Hum Reprod. 2016;31(5):926–37. https://doi.org/10.1093/humrep/dew027.

Xie J, Yang Y, Zhuo A, Gao M, Tang L, XiaoFu YX. Exosomes derived from mesenchymal stem cells attenuate nlrp3-related pyroptosis in autoimmune premature ovarian insufficiency via the nf-κb pathway. Reprod Biomed Online. 2024;48(6):103814. https://doi.org/10.1016/j.rbmo.2024.103814.

Yang M, Lin L, Sha C, Li T, Zhao D, WeiZhu HX. Bone marrow mesenchymal stem cell-derived exosomal mir-144-5p improves rat ovarian function after chemotherapy-induced ovarian failure by targeting pten. Lab Invest. 2020;100(3):342–52. https://doi.org/10.1038/s41374-019-0321-y.

Yang Y, Tang L, Xiao Y, Huang W, Gao M, XieFu JX. Mir-21-5p-loaded bone mesenchymal stem cell-derived exosomes repair ovarian function in autoimmune premature ovarian insufficiency by targeting msx1. Reprod Biomed Online. 2024;48(6):103815. https://doi.org/10.1016/j.rbmo.2024.103815.

Yin N, Luo C, Wei L, Yang G, Bo L, Mao C. The mechanisms of microrna 21 in premature ovarian insufficiency mice with mesenchymal stem cells transplantation : the involved molecular and immunological mechanisms. J Ovarian Res. 2024;17(1):75. https://doi.org/10.1186/s13048-024-01390-8.

Yin Y, Li H, Qin Y, Chen T, Zhang Z, LuShen GM. Moxibustion mitigates mitochondrial dysfunction and nlrp3 inflammatory activation in cyclophosphamide-induced premature ovarian insufficiency rats. Life Sci. 2023;314:121283. https://doi.org/10.1016/j.lfs.2022.121283.

Yu P, Zhang X, Liu N, Tang L, Peng C, Chen X. Pyroptosis: mechanisms and diseases. Signal Transduct Target Ther. 2021;6(1):128. https://doi.org/10.1038/s41392-021-00507-5.

Zheng Z, Bian Y, Zhang Y, Ren G, Li G. Metformin activates ampk/sirt1/nf-κb pathway and induces mitochondrial dysfunction to drive caspase3/gsdme-mediated cancer cell pyroptosis. Cell Cycle. 2020;19(10):1089–104. https://doi.org/10.1080/15384101.2020.1743911.

Zhuang J, Hang R, Sun R, Ding Y, Yao X, HangBai RL. Multifunctional exosomes derived from bone marrow stem cells for fulfilled osseointegration. Front Chem. 2022;10:984131. https://doi.org/10.3389/fchem.2022.984131.